We are IntechOpen,
the world's leading publisher of
Open Access books
Built by scientists, for scientists

6,900
Open access books available

186,000
International authors and editors

200M
Downloads

Our authors are among the

154
Countries delivered to

TOP 1%
most cited scientists

12.2%
Contributors from top 500 universities

CLARIVATE ANALYTICS
BOOK CITATION INDEX
INDEXED

WEB OF SCIENCE™

Selection of our books indexed in the Book Citation Index
in Web of Science™ Core Collection (BKCI)

Interested in publishing with us?
Contact book.department@intechopen.com

Numbers displayed above are based on latest data collected.
For more information visit www.intechopen.com

Chapter

Nonlinear Control Strategies of an Autonomous Double Fed Induction Generator Based Wind Energy Conversion Systems

Nouha Bouchiba, Souhir Sallem, Mohamed Ben Ali Kammoun, Larbi Chrifi-Alaoui and Saïd Drid

Abstract

In the last few decades, among the wide range of renewable energy sources, wind energy is widely used. Variable speed wind energy conversion systems based on double fed induction generator have a considerable interest mostly in case of islanded networks and/or isolated applications. In this paper, as a means to supply remote areas, an investigation of a wind energy conversion system (WECS) based on a double fed induction generator (DFIG) is carried out. The presence of both wind turbine aerodynamics and DFIG coupled dynamics causes strong nonlinearities in the studied system. Wind speed and demanded power variations have a major impact on the quality of the produced energy. In order to control and maintain the stator output voltage and frequency at their nominal values (220 V/50 Hz) under wind speed and load variations, this work presents a study of three kinds of controllers: PI, Back-Stepping and Sliding Mode controllers. These controllers are integrated in the studied system and a comparison of their dynamic performances has been developed. Moreover, in order to ensure the rotor side converter safety on the one hand and to guarantee an optimal operation of the DFIG on the other hand, a management strategy is proposed in this work. Simulation results are performed using Matlab/Simulink environment and show the effectiveness and the accuracy of each controller compared to others mainly with the presence of wind speed and load demand variations.

Keywords: wind energy conversion system, double fed induction generator, PI controller, back-stepping controller, sliding mode controller

1. Introduction

Over the past two decades, one of the most important aspects of our life is electrical energy [1, 2]. Currently, to supply power for a modern life as well as to avoid environmental issues originating from fossil fuels exploitations, the production of clean energy has become the primary objective of major universal power producing nations [3, 4]. Solar energy, wind power, biomass and geothermal are the most useful renewable energy sources [5–7]. Nowadays, wind power has become a crucial renewable energy source [8–10].

To convert wind energy into electric power, many kinds of generator concepts have been used [11, 12]. Previously, the squirrel cage induction generator was basically used in wind energy conversion system [13]. This technology is well known in fixed speed applications. Recently, the technology moves towards variable speed wind energy conversion systems [14].

Thanks to its advantages such as four quadrant power capabilities, variable speed operation, improved efficiency, decoupled regulation and reduced losses, the Doubly Fed Induction Generator DFIG has been extensively used in wind energy conversion systems WECS [1, 12, 15, 16].

In fact, using this concept, the electronic power converters are designed only at 25 to 30% of the generator capacity [12]. Therefore, from an economic point of view, this technology is more attractive compared to others (PMSG) [9, 11, 17]. Moreover, a study demonstrates that the DFIG topology presents 50% of the wind power market [10, 15].

Instead of DFIG based WECS in grid connected operation mode, a very little consideration has been paid towards the stand-alone strategy where consumers are totally disconnected from the distribution network [12]. However, in the last few decades, the availability of electricity problem in remote areas has created opportunities to exploit renewable energy sources to feed isolated loads [15]. Therefore, the implementation of stand-alone or isolated power systems can handle the rural electrification for small or medium power consumers located far from the distribution grid by providing sustainable and reliable energy supply [10, 15, 18].

Owing to the large extension of the doubly fed induction generator in isolated power systems as a primary power source generator for handling the electrification requirements of numerous isolated consumers worldwide, stand-alone wind power systems based on DFIG have become one of the most promising used technologies [10, 15]. From this perspective, the modeling and the control of WECS based DFIG have attracted extensive research efforts [2, 10, 15, 16].

Under variations of wind speed and power demand, the stator output voltage and frequency are no longer constant [12]. Highly fluctuating and unpredictable wind generation can have consequences in terms of system stability and robustness [19]. In fact, the DFIG based on WECS has strong nonlinearities [20] and the stability of power system is confronted to new challenges [21]. Many kinds of control strategies are studied and developed in literature [3, 5, 8, 10, 15].

In [8], the vector control strategy is used for the purpose of control both the active and reactive powers. In fact, to ensure the optimal operation mode, a strategy based on Adaptive fuzzy gain scheduling of the PI controller is developed.

In [10], the application of the DFIG for an isolated wind power system is examined to supply the remote area using Double-fed Induction Generator. The objective of this study is to supply different loads such as balanced, unbalanced and nonlinear loads. This study investigates the application stator/load side converter for load harmonics mitigation in the studied system. The shunt active power filter function is added to the convention control scheme of the load/stator-front voltage source converter so as to improve load harmonics. A simple technique for rotor side converter is invested to regulate Voltage and Frequency at stator/load terminals.

In [15], authors developed a speed-sensor less control strategy for a stand-alone doubly fed induction generator supplying energy to an isolated load. This technique is based on the root mean square (rms) detection. This developed direct voltage control method is applicable for not only the balanced and unbalanced load but also for standalone and grid connected mode. The control of load side converter is beyond the scope of this paper and only a diode rectifier is used for the purpose.

In [18], using fuzzy PI controller, the authors have described a control strategy for variable speed wind turbine based on DFIG. The main goal of this work is to analyze, apply and compare two kinds of controllers such as classical and Fuzzy PI.

In [19], a technique of terminal voltage build-up and the control of a stand-alone WECS based on DFIG is described. This technique is based mainly on the pitch control of the wind turbine. The active and reactive output powers are controlled and maintained equal to their reference values under sudden perturbations of wind speed and/or load variations.

In this chapter, an improved structure of a variable speed stand-alone WECS based on DFIG is proposed. In this context, a general model of the wind turbine is displayed. A detailed analysis of the autonomous DFIG for transient stability analysis is performed. The main goal of the present work is to control the stator outputs voltage and frequency as well as to maintain them within permissible operational limits (220 V/50 Hz) under wind speed and load demand variations on the one hand and to ensure the rotor side converter security on the other hand. Accordingly, to achieve these purposes, three types of controllers have been explored, modeled and integrated into the global system: The classical PI controller, a Back-Stepping and a Sliding mode controller. Besides, a management strategy is suggested to guarantee the rotor side power under 30% of the DFIG nominal power. The implementation of the overall system and different controller designs with the management strategy is achieved using Matlab/Simulink environment. In fact, simulation performances analysis of the stand-alone DFIG based WECS using the classical PI controller, back-stepping and sliding mode controllers are exhibited and discussed. A comparison between different controller process performances under sudden variation of load and wind speed disturbances is presented.

The remaining parts of this paper are organized as follows. Section 2 depicts different system component models. Section 3 describes various controller designs. Section 4 highlights the controllers management strategy. Section 5 demonstrates and compares simulation results of used controllers. Finally, Section 6 presents some drawn conclusions.

2. System modeling

The simplified schematic of the studied system is shown in **Figure 1**. It consists of a stand-alone double fed induction generator driven by a variable speed wind turbine through a gearbox. The stator of the machine is directly connected to an isolated three phase resistive inductive load (R_{Lp}, L_{Lp}). In fact, in order to make the stator outputs voltage and frequency independent from the load demand changes as well as the rotational speed variations, the rotor of the machine is supplied through a rotor side controller followed by a rotor side converter. The modeling of different components is presented and explained subsequently.
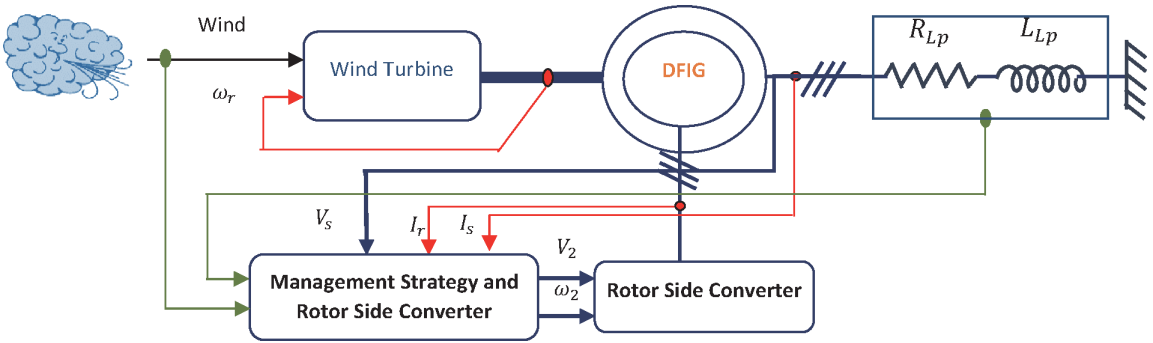

Figure 1.
Block diagram of the autonomous WECS based on DFIG.

2.1 Wind turbine model

The wind turbine aerodynamic modeling can be determined based on the power speed characteristics [12]. The mathematical expression of the mechanical power from wind turbine to the aerodynamic rotor is set forward (Eq. (1)).

$$P_m = \frac{1}{2} \rho \, R \, C_p \, (\lambda, \beta) V^3 \tag{1}$$

The power coefficient can be expressed in terms of the tip speed ratio and the pitch angle as follows (Eq. (2)):

$$C_p(\lambda, \beta) = C_1 \left(\frac{C_2}{\lambda_i} - C_3 \beta - C_4 \right) e^{\frac{-C_5}{\lambda_i}} + C_6 \lambda_i \tag{2}$$

Where the power coefficients are C_1 = 0.5176, C_2 = 116, C_3 = 0.4, C_4 = 5, C_5 = 21, C_6 = 0.0068 [12].
λ_i can be expressed by the following equation (Eq. (3)):

$$\frac{1}{\lambda_i} = \frac{1}{\lambda + 0.08\beta} - \frac{0.035}{\beta^3 + 1} \tag{3}$$

The tip speed ratio is given by (Eq. (4)):

$$\lambda = \frac{R\Omega_t}{V} \tag{4}$$

The aerodynamic torque, the generator torque and mechanical speed appearing on the shaft of the generator [11, 12] are represented respectively by (Eq. (5)–(7)).

$$C_{aer} = \frac{P_m}{\Omega_t} \tag{5}$$

$$C_m = \frac{C_{aer}}{G} \tag{6}$$

$$\Omega_t = \frac{\Omega_{mec}}{G} \tag{7}$$

In fact, the power of the used generator is low, the use of the pitch control can increase the cost of the whole system. Therefore, in this work, the pitch control does
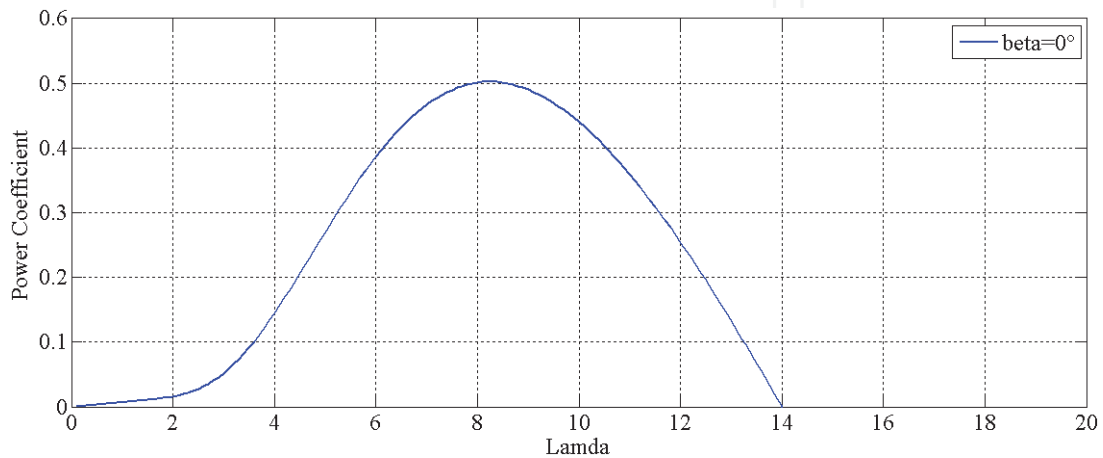

Figure 2.
Power coefficient for a pitch angle β = 0.

not prove to be a relevant solution to achieve our purpose and consequently, the pitch angle is maintained fixed ($\beta = 0$), which is a valid hypothesis for low and medium wind speeds [9]. **Figure 2** illustrates the power coefficient C_p variation versus the tip speed ratio λ for a specific chosen value of the pitch angle $\beta = 0$.

2.2 Standalone DFIG model

In this section, we attempt to analyze properly the DFIG in autonomous mode. The modeling of the three phase DFIG is carried out in a (d, q) reference frame. Using the generator convention, the Park model of the DFIG describing the functioning of this machine [22] in both stator and rotor side is given below respectively (Eqs. (8) and (9)):

$$
\begin{cases}
\dfrac{d}{dt}\psi_{sd} = -R_s I_{sd} - V_{sd} + \omega_1 \psi_{sq} \\
\dfrac{d}{dt}\psi_{sq} = -R_s I_{sq} - V_{sq} - \omega_1 \psi_{sd}
\end{cases}
\tag{8}
$$

$$
\begin{cases}
\dfrac{d}{dt}\psi_{rd} = -R_r I_{rd} + V_{rd} + \omega_2 \psi_{rq} \\
\dfrac{d}{dt}\psi_{rq} = -R_r I_{rq} + V_{rq} - \omega_2 \psi_{rd}
\end{cases}
\tag{9}
$$

As the d and q axis are magnetically decoupled, stator and rotor machine flux are expressed as (Eqs. (10) and (11)):

$$
\begin{cases}
\psi_{sd} = L_s I_{sd} + M I_{rd} \\
\psi_{sq} = L_s I_{sq} + M I_{rq}
\end{cases}
\tag{10}
$$

$$
\begin{cases}
\psi_{rd} = L_r I_{rd} + M I_{sd} \\
\psi_{rq} = L_r I_{rq} + M I_{sq}
\end{cases}
\tag{11}
$$

While functioning as a generator, the electromagnetic torque produced by the DFIG can be represented in terms of stator and rotor currents and flux as follows (Eq. (12)):

$$
C_{em} = \frac{3}{2} p \frac{M}{L_s} \left(I_{rd} \psi_{sq} - I_{rq} \psi_{sd} \right)
\tag{12}
$$

Neglecting the machine viscous friction phenomenon, the electromechanical equation is given by (Eq. (13)):

$$
\frac{dw_r}{dt} = \frac{p}{J} \left(C_m - C_{em} \right)
\tag{13}
$$

2.3 Load model

In stand-alone technology of DFIG based WECS, the stator of the machine is not connected to the grid but supplies an isolated load. Different kinds and values of loads can be connected to the stator terminals. The connected load is detected (R_{LP}, L_{LP}) in the following work. This couple (R_{LP}, L_{LP}) depends mainly on load demand power percentage noted LP_d [12]. Based on LP_d, the connecting load can be computed using the following equations (Eq. (14) and (15)).

$$R_{LP} = \frac{3V_{1n}^2}{LP_d.P_{1n}\sqrt{1 + (tg\varphi^2)}} \tag{14}$$

$$L_{LP} = \frac{R_{LP}tg\varphi}{\omega_{1n}} \tag{15}$$

Where P_{1n}, V_{1n}, and w_{1n} represent respectively nominal power, voltage and pulsation of the machine.

Electrical equations on the stator side can be rewritten as follows (Eq. (16)) [12]:

$$\begin{cases} V_{sd} = R_{LP}i_{sd} + L_{LP}\dfrac{d}{dt}i_{sd} - \omega_1 L_{LP}i_{sq} \\[2mm] V_{sq} = R_{LP}i_{sq} + L_{LP}\dfrac{d}{dt}i_{sq} + \omega_1 L_{LP}i_{sd} \end{cases} \tag{16}$$

2.4 Converter model

For the considered power schema shown in **Figure 1**, the voltages across a, b, c rotor weddings of the DFIG are constructed as follows (Eq. (17)) [17].

$$\begin{bmatrix} V_{an} \\ V_{bn} \\ V_{cn} \end{bmatrix} = \frac{V_{dc}}{3} \begin{bmatrix} 2 & -1 & -1 \\ -1 & 2 & -1 \\ -1 & -1 & 2 \end{bmatrix} \begin{bmatrix} f_1 \\ f_2 \\ f_3 \end{bmatrix} \tag{17}$$

Where f_1, f_2 and f_3 represent the control signals and V_{dc} is the DC-link voltage referring to [17].

3. Controllers synthesis

The target of the proposed DFIG based WECS control is to keep the stator voltage amplitude and frequency constant and equal to their nominal values namely 220 V and 50Hz versus the load variations and wind speed fluctuations. Accordingly, the integration of a controller inside the studied system seems crucial. A few technologies about voltage and frequency control in an autonomous system based on DFIG are studied in literature [15]. However, in terms of complexity, these techniques exhibit many disadvantages in practice. In this work, we attempt to explore three types of controllers. In a first step, the implementation of the classical PI control technique is presented. Then, thanks to its advantages, the Back-Stepping controller is modeled and integrated into the system. Finally, a new technique of control is studied known as Sliding Mode controller.

In addition, the synthesis of different control strategies is based on choosing a synchronously dq reference frame with the stator voltage that is oriented with the d axis [23]. Consequently, we can formulate (Eq. (18)):

$$\begin{cases} \boldsymbol{V_{sd} = 0} \\ \boldsymbol{V_{sq} = V_s} \end{cases} \tag{18}$$

3.1 PI controller parameters calculation

In order to ensure the convergence conditions of the proposed system and to obtain good responses, PI controller parameters should be chosen properly. This
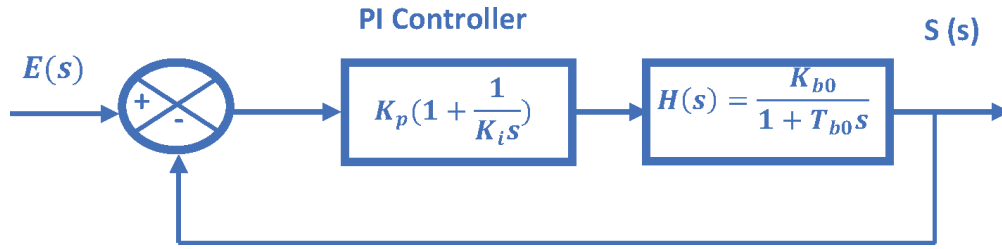
Figure 3.
The control diagram.

section describes a simple method for PI parameters computing. In general, the control diagram is presented as shown in **Figure 3**.

Where $H(s)$ represents the transfer function of the system which is given by (Eq. (19)):

$$H(s) = \frac{K_{b0}}{1 + T_{b0}s} \tag{19}$$

K_p and K_i are the PI controller parameters for proportional and integral actions respectively. These parameters are computed based on DFIG parameters so as to ensure quick and convergent response of the DFIG based WECS subsystems. K_i is determined using the pole compensation method and K_p is deduced so as to ensure a fast response of the DFIG subsystems.

3.2 PI controller design

The main principle of the PI control topology is to control and regulate different physical parameters of the system using closed loops control. In this context, while applying this controller, in order to obtain the final control signals (U_{rd} and U_{rq}), two control loops are required. The computing of reference rotor currents (I_{rd} and I_{rq}) is carried out in a first step based on the calculation of the difference between reference and measured value of stator voltage (U_{sd} and U_{sq}). Calculating the output rotor voltages is performed in a second step by minimizing the error between reference and measured rotor currents already calculated in the first step. Therefore, stator and rotor voltages can be reformulated as follows (Eq. (20) and (21)):

$$\begin{cases} V_{sd} = \left[R_sI_{sd} + L_s\dfrac{dI_{sd}}{dt} - \omega_sL_sI_{sq}\right] + M\dfrac{dI_{rd}}{dt} - \omega_1MI_{rq} \\[2mm] V_{sq} = \left[R_sI_{sq} + L_s\dfrac{dI_{sq}}{dt} + \omega_sL_sI_{sd}\right] + M\dfrac{dI_{rq}}{dt} + \omega_1MI_{rd} \end{cases} \tag{20}$$

$$\begin{cases} V_{rd} = R_rI_{rd} + L_r\dfrac{dI_{rd}}{dt} + M\dfrac{dI_{sd}}{dt} - \omega_2L_rI_{rq} - \omega_2MI_{sq} \\[2mm] V_{rq} = R_rI_{rq} + L_r\dfrac{dI_{rq}}{dt} + M\dfrac{dI_{sq}}{dt} + \omega_2L_rI_{rd} + \omega_2MI_{sd} \end{cases} \tag{21}$$

The orientation of stator voltages with the d axis leads to (Eq. (22)):

$$\begin{cases} 0 = R_sI_{sd} + L_s\dfrac{dI_{sd}}{dt} + M\dfrac{dI_{rd}}{dt} - \omega_1L_sI_{sq} - \omega_1MI_{rq} \\[2mm] V_s = R_sI_{sq} + L_s\dfrac{dI_{sq}}{dt} + M\dfrac{dI_{rq}}{dt} + \omega_1L_sI_{sd} + \omega_1MI_{rd} \end{cases} \tag{22}$$

Departing from these equations and omitting coupling terms, reference rotor currents can be expressed in terms of stator voltages.

Moreover, referring to (Eq. (22)), the first derivative of the stator current can be written as (Eq. (23)):

$$
\begin{cases}
\dfrac{dI_{sd}}{dt} = \dfrac{1}{L_s}\left[-R_s I_{sd} - M\dfrac{dI_{rd}}{dt} + \omega_1 L_s I_{sq} + \omega_1 M I_{rq}\right] \\[3mm]
\dfrac{dI_{sq}}{dt} = \dfrac{1}{L_s}\left[V_s - R_s I_{sq} - M\dfrac{dI_{rq}}{dt} - \omega_1 L_s I_{sd} - \omega_1 M I_{rd}\right]
\end{cases}
\tag{23}
$$

Referring to (Eq. (21)) and (Eq. (23)), reference rotor voltages are given as (Eq. (24)):

$$
\begin{cases}
V_{rd} = R_r I_{rd} - \omega_2 L_r I_{rq} - \omega_2 M I_{sq} + L_r \dfrac{dI_{rd}}{dt} + \dfrac{M}{L_s} L_d \\[3mm]
V_{rq} = R_r I_{rq} + \omega_2 L_r I_{rd} + \omega_2 M I_{sd} + L_r \dfrac{dI_{rq}}{dt} + \dfrac{M}{L_s} L_q
\end{cases}
\tag{24}
$$

Where

$$
\begin{cases}
L_d = \left[-R_s I_{sd} - M\dfrac{dI_{rd}}{dt} + \omega_1 L_s I_{sq} + \omega_1 M I_{rq}\right] \\[3mm]
L_q = \left[V_s - R_s I_{sq} - M\dfrac{dI_{rq}}{dt} - \omega_1 L_s I_{sd} - \omega_1 M I_{rd}\right]
\end{cases}
$$

(Eq. (24)) can be rewritten as follows:

$$
\begin{cases}
V_{rd} = \left[R_r I_{rd} + \left(L_r - \dfrac{M^2}{L_s}\right)\dfrac{dI_{rd}}{dt}\right] + T_d \\[3mm]
V_{rq} = \left[R_r I_{rq} + \left(L_r - \dfrac{M^2}{L_s}\right)\dfrac{dI_{rq}}{dt}\right] + T_q
\end{cases}
\tag{25}
$$

Where

$$
\begin{cases}
T_d = -\left(\omega_2 L_r - \dfrac{M^2}{L_s}\omega_1\right)I_{rq} - M(\omega_2 - \omega_1)I_{sq} - \dfrac{R_s M}{L_s}I_{sd} \\[3mm]
T_q = \left(\omega_2 L_r - \dfrac{M^2}{L_s}\omega_1\right)I_{rd} + M(\omega_2 - \omega_1)I_{sd} - \dfrac{R_s M}{L_s}I_{sq} + \dfrac{M}{L_s}V_s
\end{cases}
$$

3.3 Backstepping controller design

In this paper, we aim at improving performances of the studied system. In this context, in order to answer this need and to respond to our objective, we are basically interested in developing control strategies resting on linearization of the autonomous WECS based DFIG.

With the presence of many kinds of uncertainties, the back-stepping controller is able to linearize effectively a nonlinear system. In fact, during stabilization, unlike other techniques of linearization, this control technique has the flexibility to keep useful nonlinearities [23].

The stabilization of the virtual control state stands for the main purpose of the Backstepping controller. Therefore, this control strategy rests on the stabilization of a variable error by selecting carefully the suitable control inputs which are obtained from the analysis of Lyapunov function [24, 25].

In order to regulate effectively the output reference rotor voltages, the reference rotor currents are obtained based on a PI controller. Then, the rotor voltages are obtained by using a back-stepping controller.

Indeed, the first step of the Backstepping control is meant to identify the tracking errors by Eq. (26).

$$\begin{cases} e_1 = I_{rd}^* - I_{rd} \\ e_2 = I_{rq}^* - I_{rq} \end{cases} \tag{26}$$

Tracking errors first derivative can be written as Eq. (27):

$$\begin{cases} \dot{e}_1 = \dot{I}_{rd}^* - \dot{I}_{rd} \\ \dot{e}_2 = \dot{I}_{rq}^* - \dot{I}_{rq} \end{cases} \tag{27}$$

The derivative of the rotor currents can be obtained referring to Eq. (24) and can be written as follows (Eq. (28)):

$$\begin{cases} \dfrac{dI_{rd}}{dt} = \dfrac{V_{rd}}{L_r} - \dfrac{R_r}{L_r} I_{rd} - \dfrac{M}{L_r} \dfrac{dI_{sd}}{dt} + \omega_2 I_{rq} + \omega_2 \dfrac{M}{L_r} I_{sq} \\ \dfrac{dI_{rq}}{dt} = \dfrac{V_{rq}}{L_r} - \dfrac{R_r}{L_r} I_{rq} - \dfrac{M}{L_r} \dfrac{dI_{sq}}{dt} - \omega_2 I_{rd} - \omega_2 \dfrac{M}{L_r} I_{sd} \end{cases} \tag{28}$$

To ensure the convergence and the stability of the system, the Lyapunov function is chosen to be a quadratic function (defined as a positive function) and is given by Eq. (29).

$$V_1 = \frac{1}{2} e_1^2 + \frac{1}{2} e_2^2 \tag{29}$$

The expression of Lyapunov derivative function is defined as negative function and it is expressed as follows (Eq. (30)).

$$\dot{V}_1 = -K_1 e_1^2 - K_2 e_2^2 \tag{30}$$

Eq. (29) can be rewritten as:

$$\dot{V}_1 = e_1 \dot{e}_1 + e_2 \dot{e}_2 \tag{31}$$

In order to guarantee a stable tracking, the Back-stepping gain coefficients K_1 and K_2 need to be positive [25].

Referring to Eqs. (30) and (31), it can be concluded that (Eq. (32)):

$$\begin{cases} e_1 \dot{e}_1 = -K_1 e_1^2 \\ e_2 \dot{e}_2 = -K_2 e_2^2 \end{cases} \tag{32}$$

Consequently, we can obtain (Eq. 33):

$$\begin{cases} -K_1 e_1 = \dot{I}_{rd}^* - \dot{I}_{rd} \\ \\ -K_2 e_2 = \dot{I}_{rq}^* - \dot{I}_{rq} \end{cases} \qquad (33)$$

Based on Eqs. (28) and (33), we can obtain (Eq. (34)):

$$\begin{cases} -K_1 e_1 = \dot{I}_{rd}^* - \dfrac{V_{rd}}{L_r} + \dfrac{R_r}{L_r} I_{rd} + \dfrac{M}{L_r} \dfrac{dI_{sd}}{dt} - \omega_2 I_{rq} - \omega_2 \dfrac{M}{L_r} I_{sq} \\ \\ -K_2 e_2 = \dot{I}_{rq}^* - \dfrac{V_{rq}}{L_r} + \dfrac{R_r}{L_r} I_{rq} + \dfrac{M}{L_r} \dfrac{dI_{sq}}{dt} + \omega_2 I_{rd} + \omega_2 \dfrac{M}{L_r} I_{sd} \end{cases} \qquad (34)$$

Finally, the rotor control voltages are given by (Eq. (35)):

$$\begin{cases} V_{rd} = L_r \left[K_1 e_1 + \dot{I}_{rd}^* + \dfrac{R_r}{L_r} I_{rd} + \dfrac{M}{L_r} \dfrac{dI_{sd}}{dt} - \omega_2 I_{rq} - \omega_2 \dfrac{M}{L_r} I_{sq} \right] \\ \\ V_{rq} = L_r \left[K_2 e_2 + \dot{I}_{rq}^* + \dfrac{R_r}{L_r} I_{rq} + \dfrac{M}{L_r} \dfrac{dI_{sq}}{dt} + \omega_2 I_{rd} + \omega_2 \dfrac{M}{L_r} I_{sd} \right] \end{cases} \qquad (35)$$

3.4 Sliding mode controller design

Thanks to its advantages such as the simplicity of the implementation, the stability and the insensitivity to external disturbances, the sliding mode controller is a widely used strategy [26]. Similar to the back-stepping controller, the aim of this strategy is to stabilize a chosen virtual control state. It rests on the stabilization of a variable error, defined as a sliding surface, by selecting the suitable control inputs. In fact, the output control parameters are obtained by the determination of two components: U^{eq} and U^N as given in Eq. (36).

In this section, a detailed analysis of this controller is presented in order to obtain the control output rotor voltages which regulate the output voltage and frequency of the system and maintain them constant no matter which external disturbances occur.

$$\begin{cases} V_{rd} = V_{rd}^{eq} + V_{rd}^N \\ \\ V_{rq} = V_{rq}^{eq} + V_{rq}^N \end{cases} \qquad (36)$$

In our research, the sliding surface is chosen as follows (Eq. (37)):

$$\begin{cases} S_1 = I_{rd}^* - I_{rd} \\ \\ S_2 = I_{rq}^* - I_{rq} \end{cases} \qquad (37)$$

The derivative of sliding surfaces is given by (Eq. (38)):

$$\begin{cases} \dot{S}_1 = \dot{I}_{rd}^* - \dot{I}_{rd} \\ \\ \dot{S}_2 = \dot{I}_{rq}^* - \dot{I}_{rq} \end{cases} \qquad (38)$$

Based on Eq. (28), Eq. (38) can be rewritten as follows (Eq. (39)):

$$
\begin{cases}
\dot{S}_1 = \dot{I}_{rd}^* - \dfrac{V_{rd}}{L_r} + \dfrac{R_r}{L_r}I_{rd} + \dfrac{M}{L_r}\dfrac{dI_{sd}}{dt} - \omega_2 I_{rq} - \omega_2 \dfrac{M}{L_r}I_{sq} \\
\dot{S}_2 = \dot{I}_{rq}^* - \dfrac{V_{rq}}{L_r} + \dfrac{R_r}{L_r}I_{rq} + \dfrac{M}{L_r}\dfrac{dI_{sq}}{dt} + \omega_2 I_{rd} + \omega_2 \dfrac{M}{L_r}I_{sd}
\end{cases}
\tag{39}
$$

In a first step, and during the sliding mode, in order to compute the first part of the control signal, we can set forward these hypotheses (Eq. (40)):

$$
\begin{cases}
S = 0 \\
\dot{S} = 0 \\
V_{rd}^N = 0 \\
V_{rq}^N = 0
\end{cases}
\tag{40}
$$

Subsequently, equivalent voltage expressions are formulated as follows (Eq. (41)):

$$
\begin{cases}
V_{rd}^{eq} = L_r \left[\dot{I}_{rd}^* + \dfrac{R_r}{L_r}I_{rd} + \dfrac{M}{L_r}\dfrac{dI_{sd}}{dt} - \omega_2 I_{rq} - \omega_2 \dfrac{M}{L_r}I_{sq} \right] \\
V_{rq}^{eq} = L_r \left[\dot{I}_{rq}^* + \dfrac{R_r}{L_r}I_{rq} + \dfrac{M}{L_r}\dfrac{dI_{sq}}{dt} + \omega_2 I_{rd} + \omega_2 \dfrac{M}{L_r}I_{sd} \right]
\end{cases}
\tag{41}
$$

In a second step, during the convergence mode, to ensure the condition $S\dot{S} < 0$, we can suppose that (Eq. (42)):

$$
\begin{cases}
V_{rd}^N = K_1\, sign(S_1) \\
V_{rq}^N = K_2\, sign(S_2)
\end{cases}
\tag{42}
$$

To guarantee a stable tracking, K_1 and K_2 are chosen positive constants [27].

4. Controllers management strategy

With the rapid progress of control topologies, various nonlinear control strategies such as Backstepping and sliding mode controllers whetted the interest of many researchers who attempted to develop and further enhance them. These algorithms succeeded to improve different performances of the studied system, but they remain unable to ensure optimal and safe operation of the rotor side converter. In general, the rotor side converter integrated in a DFIG based WECS is estimated at 30% of the machine nominal power which presents the main advantage of the DFIG use [12]. However, with the presence of load demand power variations and wind speed fluctuations, the rotor demanded power may exceed 30% of the DFIG nominal power. Hence, to ensure a safe functioning of the RSC and to guarantee an optimal operation mode of the DFIG, a management strategy is proposed. The wind energy can be then used effectively in order to satisfy the demand of the connected load on the one hand and to ensure security of the DFIG rotor side converter with an optimal operation on the other hand.

Based on the captured wind velocity and the load demanded power, the proposed management algorithm computes and specifies secure operation boundaries ($0.7\,\omega_{1n} \leq \omega_r \leq 1.3\,\omega_{1n}$).
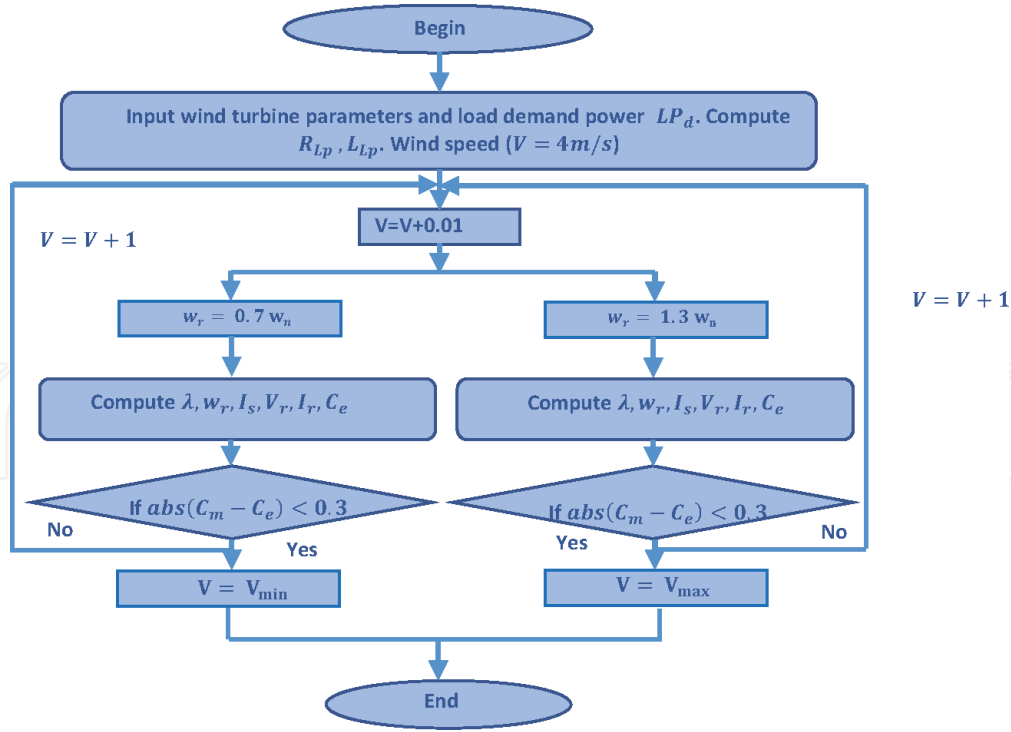
Figure 4.
Management strategy flowchart.

Thus, in order to obtain nominal stator output voltage and frequency ($V = 220V, F = 50H$), both rotor voltage and frequency change with every detected change in load demand power (Eq. (43)) to maintain a constant electromagnetic torque (Eq. (44)). As it is shown in (Eq. (43)), the rotor voltage depends mainly on the load impedance whereas, the rotor pulsation depends basically on the rotational speed of the machine.

$$\begin{cases} \overline{V}_r = \dfrac{j}{\omega_1 M} \cdot \dfrac{\overline{Z}.\overline{Z}_{sT}}{\overline{Z}_{ch}} \overline{V}_s \\ \omega_2 = \omega_1 - \omega_r \end{cases} \tag{43}$$

$$C_e = \frac{3}{2} p \frac{\overline{V}_s^2}{\omega_1} \Im\mathrm{mag} \left(j \frac{\overline{Z}_{sT}}{\overline{Z}_{ch}^2} \right) \tag{44}$$

where $\overline{Z}_{LP} = R_{LP} + j\omega_1 L_{LP}, \overline{Z}_r = R_r + j\omega_2 L_r, \overline{Z}_{sT} = (R_s + R_{LP}) + j\omega_1(L_s + L_{LP})$ and $\overline{Z} = \overline{Z}_r + \frac{\omega_1 \omega_2 M^2}{\overline{Z}_{sT}}$.

The proposed algorithm can be summarized by the flowchart displayed in **Figure 4**.

The handling of the algorithm detailed in **Figure 4** allows us towards the end to obtain the speed range for every connected load. Within this framework, the main idea of the developed strategy is to detect first the load demanded power. Based on the wind turbine parameters, the connected load value and the rotor speed limits ($w_r = 0.7w_n$ and $w_r = 1.3w_n$), the wind speed limits are calculated (V_{min} and V_{max}). Otherwise, if the detected wind speed does not respect the given algorithm boundaries, the DFIG has to disconnect from the load unless the wind speed respects computed limits.

5. Simulation results and discussion

In order to analyze the system modeling, to check performances of the studied controllers and to compare the system responses using each control strategy, the

proposed stand-alone wind energy conversion system based on doubly fed induction generator is implemented and tested using Matlab/Simulink environment.

The studied system rests on a wind turbine, a doubly fed induction generator and a three-phase isolated load. The DFIG parameters are obtained experimentally in the LTI, Cuffies-Soissons, France laboratory. They are exhibited in **Table 1** [28].

To satisfy the convergence conditions of the proposed system, parameters of PI controller, Backstepping and Sliding mode controllers are selected properly.

In this paper, our intrinsic purpose is to maintain constant output stator voltage and frequency under sudden variations of wind speed and load demand. Therefore, a selected profile of wind speed deduced from the proposed management strategy and load demand is applied to the system. These profiles are chosen properly in such a way that rotor side power is limited under 30% of DFIG nominal power so as to ensure the safety of the rotor side converter.

In fact, to analyze the system performances, a comparison between the three proposed strategies of control is carried out. A set of different simulation tests have been performed and carried out for 20 seconds.

The profile of wind speed profile is presented in **Figure 5**. To check the performance of the proposed model, different sudden variations are applied to the system. The wind speed varies from $7 m/s$ to $15.3 \, m/s$. For $15 \leq t \leq 20 s$, the wind velocity increases to attend $15.3 \, m/s$. At this moment, for safety reasons, the management and control strategy reacts in such a way it disconnects the DFIG from the load.

Figure 6 represents the demand of the isolated load. The demanded power of the load presents many variations. For $0 \leq t \leq 5 s$, the demand of the connected load is equal to the nominal power P_n. At $t = 5 s$, the demand of the load decreases and becomes $0.8 P_n$. However, at $= 10 s$, an increase in the demanded power from $0.7 P_n$ to $1.2 P_n$ is recorded. For $15 \leq t \leq 20 s$, when the wind speed increases suddenly, the load is totally disconnected from the DFIG and the power transmitted to the isolated load becomes equal to zero.

To interpret properly the different results, to demonstrate the load and the wind speed variation effects on the system response and to show the response of each controller, two zooms are chosen to be presented in different figures. A zoom noted (a) is performed at $t = 5 s$ to show the effect of the load demanded power variation. Moreover, at $t = 15 s$ a zoom noted (b) is stated in different figures in order to

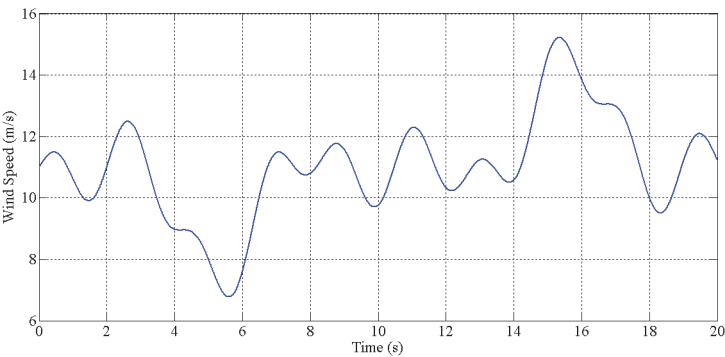| $R_s(\Omega)$	$R_r(\Omega)$	$L_s(H)$	$L_r(H)$	$M(H)$	$P(KW)$
4.9	4	0.24	0.24	0.2	1.5

Table 1.
DFIG parameters.

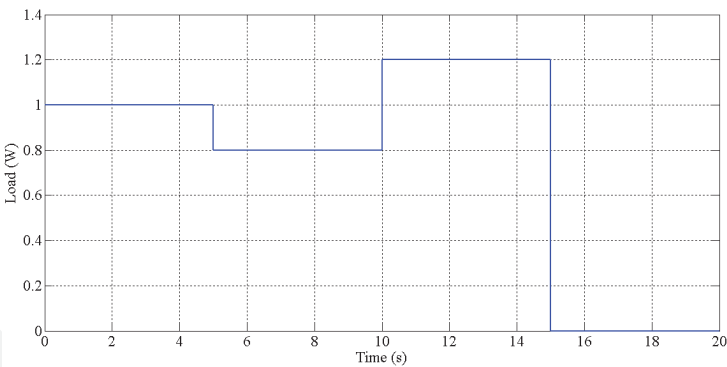
Figure 5.
Wind speed profile.

Figure 6.
Load demand variations.

demonstrate the effectiveness of the management strategy when the wind speed does not abide by computed limits.

Figure 7 plots the output stator voltages (U_{sd} and U_{sq}). We notice that the stator voltage is maintained constant in case of load demand variations (at $t = 5s$ and $t = 10\,s$) and even when a wind speed fluctuation is detected (at $t = 15s$).

Figure 8 describes the rotor voltages (U_{rd} and U_{rq}) which correspond to the control signals of the system. In each detected variation in load impedance and wind speed, controllers react by controlling rotor voltages which vary in order to maintain constant output voltage and frequency. For example, at $t = 5s$, the load demanded power changes. So, the direct rotor voltage (U_{rd}) decreases and the quadratic rotor voltage (U_{rq}) increases instantaneously to regulate the stator outputs. In fact, when the load demand varies at $t = 10s$, the control system reacts to obtain the same results
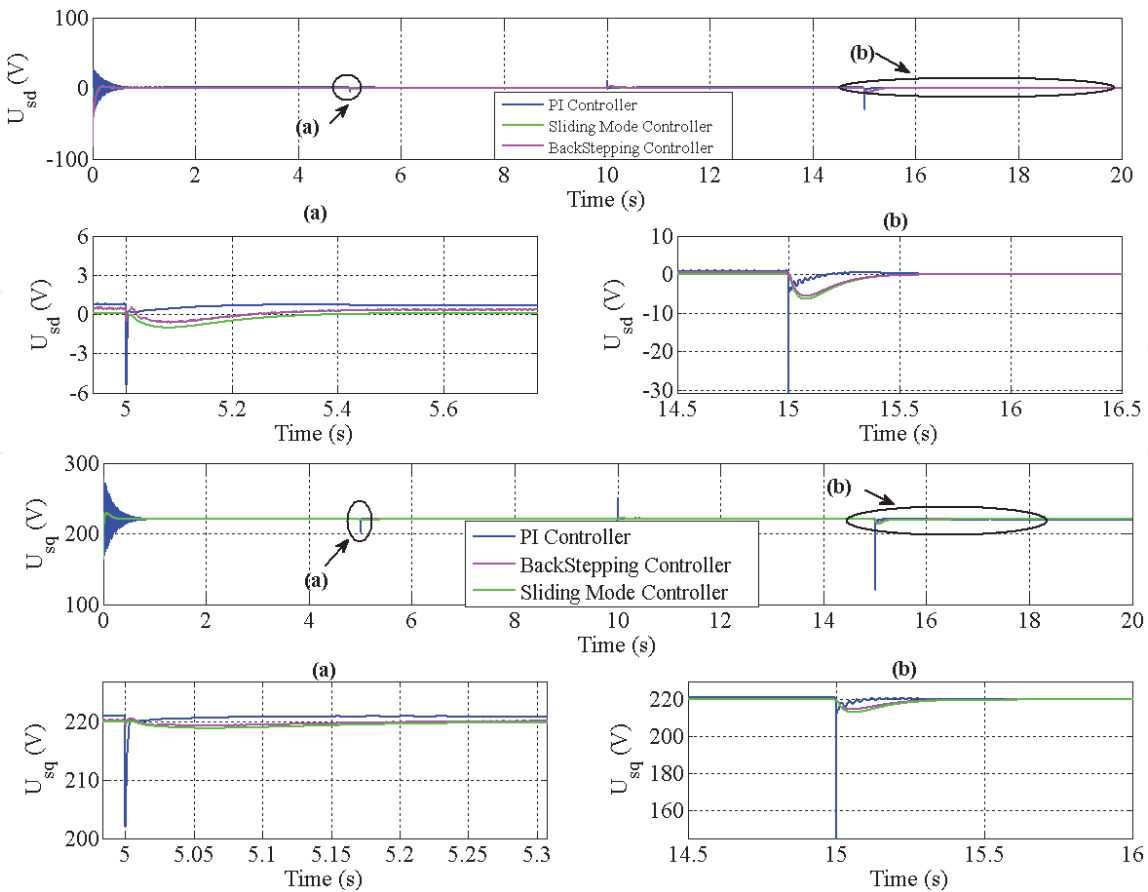

Figure 7.
The stator output voltages responses using the PI controller, the Backstepping controller and the Sliding mode controller. Two zooms are done at t = 5 s noted (a) and at t = 15 s noted (b) to see the advantages and disadvantages of each controller.
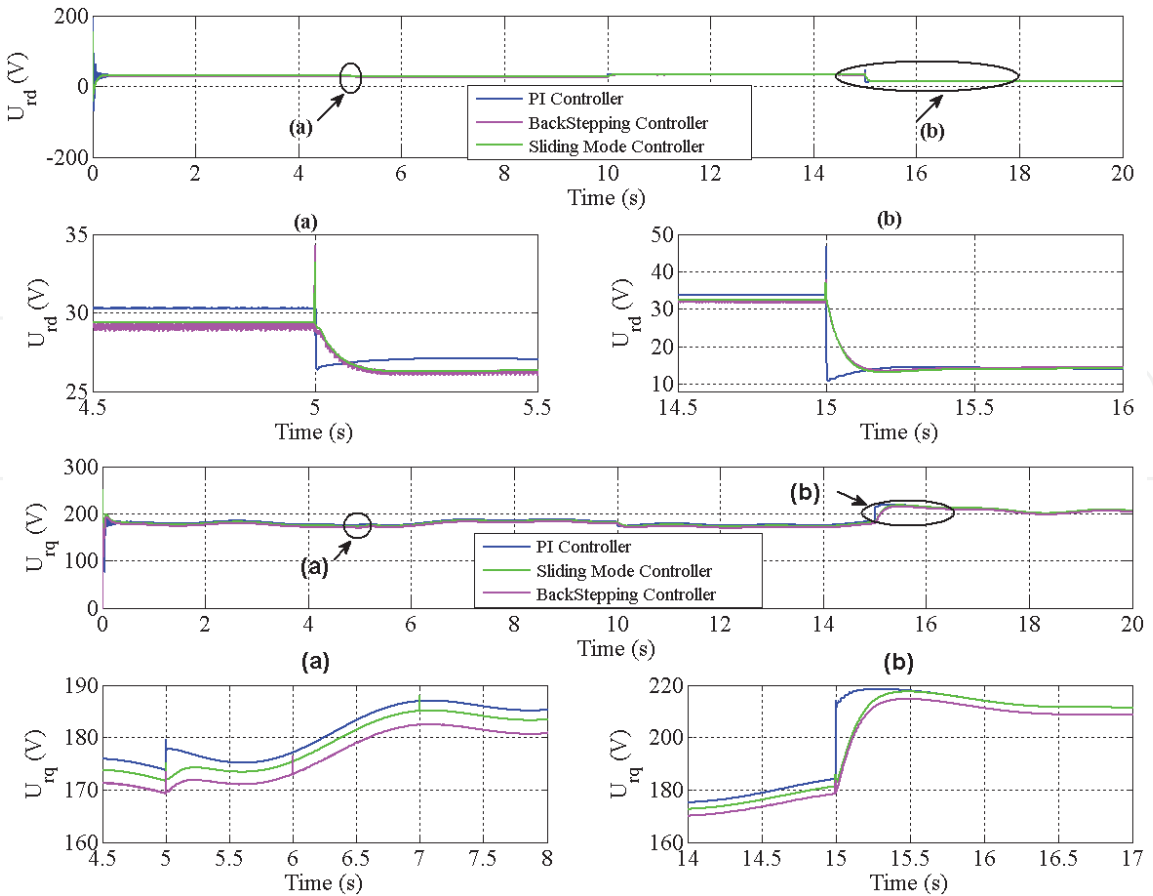
Figure 8.
The rotor output voltages responses using the PI controller, the Backstepping controller and the Sliding mode controller. Two zooms are done at t=5 s noted (a) and at t=15 s noted (b) to see the advantages and disadvantages of each controller.

in stator side. Furthermore, at $t = 0.1s$, in both **Figures 7** and **8**, we detect the existence of a transient regime uniquely in case a PI controller is used. At this starting time, some picks are presented. However, the response of the backstepping and the sliding mode controllers are smoother and more flexible. Thus, while comparing the response of the backstepping and the sliding mode controllers, it is obviously visible in **Figures 7** and **8** that the steady state regime is reached faster when the backstepping controller is used. In both **Figures 7** and **8**, the presence of two zooms (a and b) permits to check the performances of the studied system, to judge the response of each controller and to select the best one. Departing from those figures (**Figures 7(a)** and **(b)** and **8(a)** and **(b)**), in case of implementing a PI controller, we notice the presence of overshoot in stator and rotor output voltages. Thus, the robustness of the backstepping and sliding mode controllers is demonstrated.

Figure 9 highlights the evolution of the stator pulsation w_1, the rotor pulsation w_2 and the electric angular speed of the DFIG w_r. We infer that w_2 and w_r vary inversely to keep a constant stator pulsation and constant output frequency accordingly. Thus, the variation of the wind speed affects the rotor pulsation and the electric angular speed which is a normal process.

The stator output currents are displayed in **Figure 10**. It is deduced that when the power demanded by the load changes, the stator currents change in order to satisfy the demand of the load. Moreover, in zone (b), the wind speed increases and reaches $15.3 \, m/s$. Therefore, for security reasons, the management strategy reacts to disconnect the DFIG from the load and subsequently, the power supplied to the load becomes equal to zero. At this moment, the stator currents increase and become equal to zero. However, the controller operates properly, and the stator voltage remains equal to the nominal value $220 \, V$ and remains ready for the next coupling of the DFIG and the load.
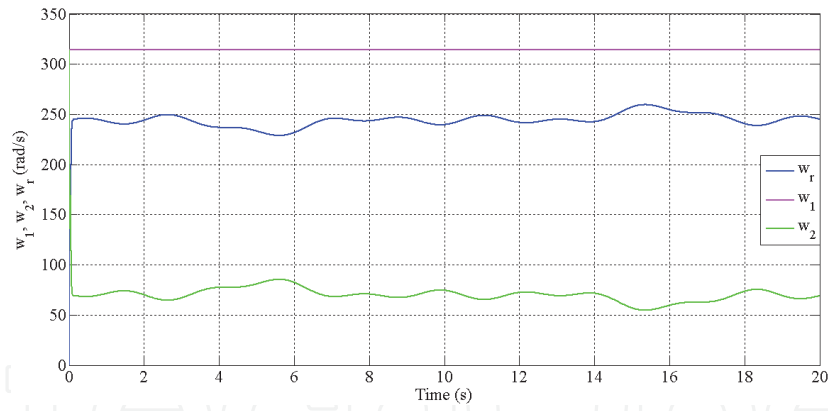
Figure 9.
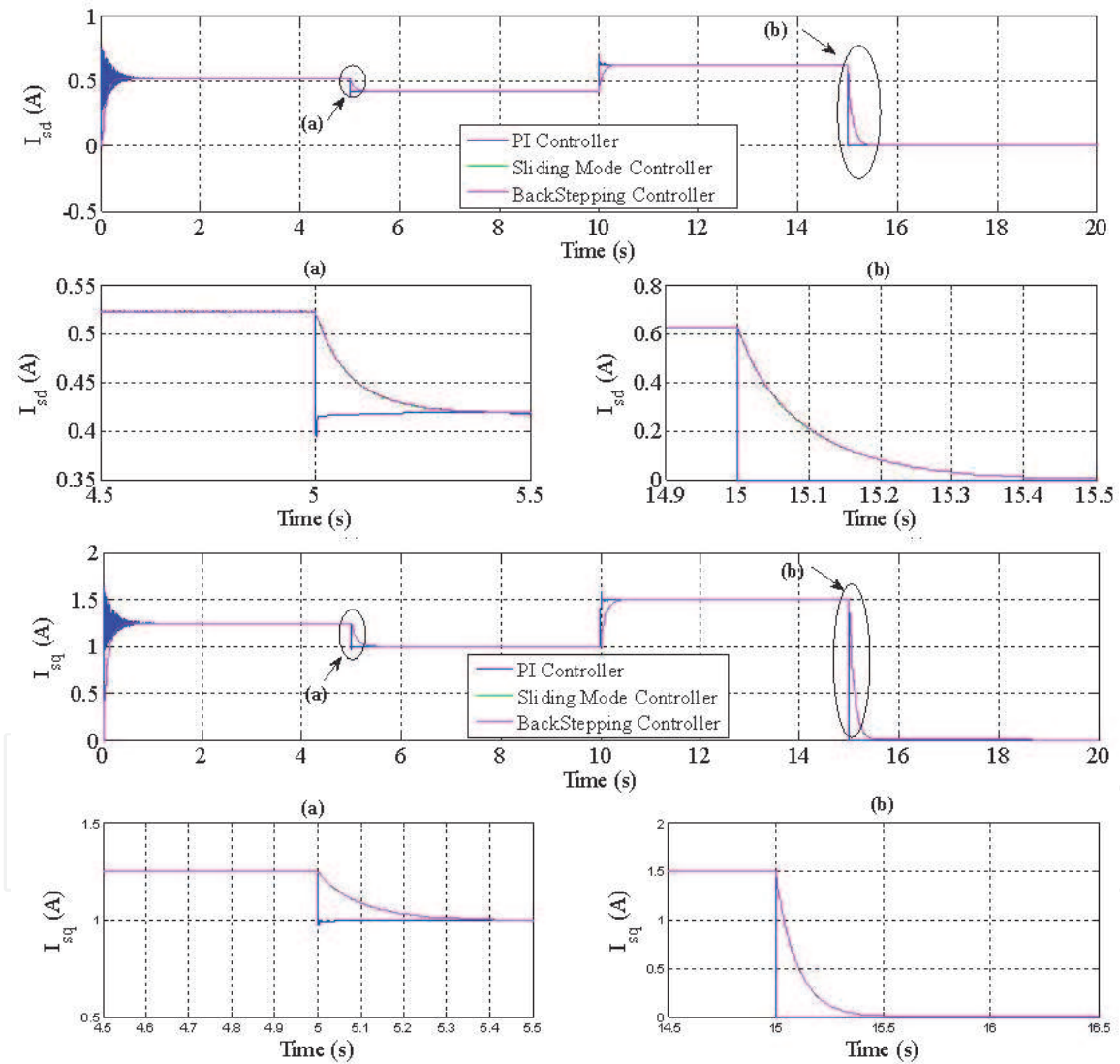*Machine pulsations.*

Figure 10.
The stator output currents responses using the PI controller, the Backstepping controller and the Sliding mode controller. Two zooms are done at t=5 s noted (a) and at t=15 s noted (b) to see the advantages and disadvantages of each controller.

A scrutiny of **Figures 8–10** reveals that, by comparing these three strategies, the results obtained by using the Backstepping and the sliding mode controllers are faster and more flexible than these obtained by using the PI control topology.

In order to evaluate developed control strategy performances for each load and wind speed variations, the RMSE (Root-Mean-Square Error) is calculated as follows:

Method	RMSE (V_{sd})	RMSE (V_{sq})
PI Controller	0.78	1.07
Backstepping Controller	0.45	0.32
Sliding mode Controller	0.11	0.09

Table 2.
V_{sd} and V_{sq} curves errors (Time = $[0s - 5s]$).

Method	RMSE (V_{sd})	RMSE (V_{sq})
PI Controller	0.64	0.87
Backstepping Controller	0.38	0.24
Sliding mode Controller	0.08	0.07

Table 3.
V_{sd} and V_{sq} curves errors (Time = $[5s - 10s]$).

Method	RMSE (V_{sd})	RMSE (V_{sq})
PI Controller	0.85	1.2
Backstepping Controller	0.55	0.36
Sliding mode Controller	0.13	0.11

Table 4.
V_{sd} and V_{sq} curves errors (Time = $[10s - 15s]$).

$$RMSE = \sqrt{\frac{1}{N} \sum_{i=1}^{N} (x_i - \overline{x_i})^2} \qquad (45)$$

Where N is the number of obtained points, $\overline{x_i}$ is the estimated value, x_i is the observed value.

Tables 2–4 sum up the RMSE of different algorithms for the same conditions (wind speed and load variations). As noticed, in each table, the RMSE of the Sliding mode controller is the smallest value. As a matter of fact, the different results obtained by this controller are close to the desired results which confirms the effectiveness of the sliding mode algorithm compared to others.

6. Conclusion

The modeling and analysis of the isolated DFIG based on WECS have been presented. The main purpose of this chapter is on the one hand to regulate the output voltage and frequency, to maintain them constant and equal to their nominal values (220 V, 50 Hz) under wind speed fluctuations and load demand variations and on the other hand to guarantee a safe operation mode of the rotor side converter through limiting the rotor side power by around 30% of the machine power. Therefore, three different system control strategies are proposed and examined. Compared to the PI controller, a stable operation of the whole system is obtained with the application of back-stepping and sliding mode controllers. However, the Sliding mode controller presents more precision and its responses are much faster than the Backstepping controller. Thus, the system performances such as precision,

stability, rapidity are improved. Analysis and simulation results prove the accuracy as well as the effectiveness of both the Back-stepping and sliding mode control strategies compared to classic control strategy.

Acknowledgements

Nomenclature

R_s resistance of a stator phase
L_s stator inductance
ψ_s stator flux
I_s stator current
V_s stator voltage
w_1 electric stator angular speed
w_r electric angular speed of the DFIG
R R is the turbine radius
V wind speed
R_r resistance of a rotor phase
L_r rotor inductance
ψ_r rotor flux
I_r rotor current
V_r rotor voltage
w_2 electric rotor angular speed
M maximum coefficient of mutual induction
ρ air density
G gain of the gearbox

Author details

Nouha Bouchiba[1]*, Souhir Sallem[1], Mohamed Ben Ali Kammoun[1],
Larbi Chrifi-Alaoui[2] and Saïd Drid[3]

1 Laboratoire Systèmes Electriques et Energies Renouvelables LSEER, National
Engineering School of Sfax (ENIS), Tunisia

2 University of Picardie Jules Verne, Cuffies, France

3 LSPIE Laboratory, University of Batna, Algeria

*Address all correspondence to: bouchibanouha@gmail.com

IntechOpen

References

[1] Ihssen Hamzaoui, Farid Bouchafaa, Abdelaziz Talha. Advanced control for wind energy conversion systems with flywheel storage dedicated to improving the quality of energy. International journal of hydrogen energy 41(2016) 20832–20846.

[2] Donghua Wang. A Novel Variable Speed Diesel Generator Using Doubly Fed Induction Generator and Its Application in Decentralised Distributed Generation Systems. Ph.D. thesis, Curtin University, School of Electrical and Computer Engineering 2012

[3] C. Evangelista, P. Puleston, F. Valenciaga. Wind turbine efficiency optimization. Comparative study of controllers based on second order sliding modes. International journal of hydrogen energy 35(2010) 5934–5939.

[4] S. Tamalouzt, N. Benyahia, T. Rekioua, D. Rekioua, R. Abdessemed. Performances analysis of WT-DFIG with PV and fuel cell hybrid power sources system associated with hydrogen storage hybrid energy system. International journal of hydrogen energy 41(2016) 21006–21021.

[5] C.A. Evangelista, F. Valenciaga, P. Puleston. Multivariable 2-sliding mode control for a wind energy system based on a double fed induction generator. International journal of hydrogen energy 37(2012)10070–10075.

[6] Mohamed Kaouane, Akkila Boukhelifa, Ahmed Cheriti. Regulated output voltage double switch Buck-Boost converter for photovoltaic energy application. International journal of hydrogen energy 41(2016)20847–20857.

[7] S. Ould Amrouche, D. Rekioua, T. Rekioua, S. Bacha. Overview of energy storage in renewable energy systems. International journal of hydrogen energy 41(2016) 20914–20927.

[8] Khouloud Bedoud, Mahieddine Ali-rachedi, Tahar Bahi, Rabah Lakel. Adaptive Fuzzy Gain Scheduling of PI Controller for control of the Wind Energy Conversion Systems. Energy Procedia 74(2015)211–225.

[9] R.Melicio, V.M.F. Mendes, J.P.S. Catalao. Comparative study of power converter topologies and control strategies for the harmonic performance of variable-speed wind turbine generator systems. Energy 36 (2011) 520–529.

[10] Rishabh Dev Shukla, Ramesh Kumar Tripathi. Isolated Wind Power Supply System using Doubl-fed Induction Generator for remote areas. Energy Conversion and Management 96 (2015) 473–489.

[11] Youcef Soufi , Sami Kahla, Mohcene Bechouat. Feedback linearization control based particle swarm optimization for maximum power point tracking of wind turbine equipped by PMSG connected to the grid. International journal of hydrogen energy 41(2016) 20950–20955.

[12] Souhir Sallem, Nouha Bouchiba, Soulayman Kammoun, Mohamed BA Kamoun. Energy management algorithm for optimum control of an off-battery autonomous DG/DFIG based WECS. The International Journal of Advanced Manufacturing Technology (2016), doi:10.1007/s00170-016-9682-1.

[13] Nouha BOUCHIBA, Souhir SALLEM, M.B.A KAMMOUN. Three-Phase Self-Excited Induction generator analysis in stand-alone mode. 6th International Renewable Energy Congress (IREC) 2015.

[14] Soro Siell_e Martin, Ahmed Chebak. Concept of educational renewable energy laboratory integrating wind,

solar and biodiesel energies. International journal of hydrogen energy 41(2016)21036–21046.

[15] Rishabh Dev Shukla, Ramesh Kumar Tripathi. A novel voltage and frequency controller for standalone DFIG based Wind Energy Conversion System. Renewable and sustainable Energy Reviews 37(2014)69–89.

[16] Gonzalo Abad, Jesus Lopez, Miguel A. Rodriguez, Luis Marrayo, Grzegorz Iwanski. Doubly Fed Induction Machine, Modeling and control for wind energy generation. IEEE Press 445 Hoes Lane, Piscatway, JJO8854.

[17] Riad Aissou, Toufik Rekioua, Djamila Rekioua, Abdelmounaı̈m Tounzi. Robust nonlinear predictive control of permanent magnet synchronous generator turbine using Dspace hardware. International journal of hydrogen energy 41(2016)21047–21056.

[18] B.Hamane, M. Benghanem, A.M. Bouzid, A. Bellabbes, M. Bouhamida, A. Draou. Control for variable speed wind turbine driving a doubly fed enduction generator using Fuzzy-PI Control. Energy Procedia 18(2012)476–485.

[19] R.K. Patnaik, P.K. Dash. Fast adaptive finite-time terminal sliding mode power control for the rotor side converter of the DFIG based wind energy conversion system. Sustainable Energy, Grids and Networks1 (2015) 63–84, 31 January 2015.

[20] F.E.V. Taveiros, L.S.Barros, F.B. Costa. Back to back converter state feedback control of DFIG (doubly fed induction generator) based wind turbines. Energy 89 (2015) 896–906,14 July 2015.

[21] Zhanfeng Song, Tingna Shi, Changliang Xia, Wei Chen. A novel adaptive control schema for dynamic performance improvement of DFIG based wind turbines. Energy 38 (2012) 104–117, 25 January 2012.

[22] Mohamed Ben Ali Kammoun. Modélisation des machines. National Engineering school of Sfax, ENIS Sfax, Tunisia.

[23] Soulaymen Kammoun. Contribution à la commande des systèmes de puissance en vue de l'intégration de l'énergie éolienne dans le réseau. Doctoral thesis 2016, National Engineering school of Sfax, ENIS Sfax, Tunisia.

[24] Badre Bossoufi, Mohammed Karim, Ahmed Lagrioui, Mohammed Taoussi, Aziz Derouich. Observer backstepping control of DFIG Generator for wind turbines variable speed: FPGA-based implementation. Renewable Energy 81 (2015) 903–97. 24 April 2015.

[25] Nihel Khemiri, Adel Khedher, Mohamed Faouei Mimouni. An adaptive nonlinear backstepping control of DFIG by wind turnines. WSEAS TRANSACTIONS on ENVIRONMENT and DEVELOPMENT. Issue 2, Volume 8, April 2012.

[26] Youcef Soufi, Sami Kahla, Mohcene Bechouat. Particle swarm optimization based sliding mode control of variable speed wind energy conversion system. International journal of hydrogen energy 41(2016) 20956–20963.

[27] V.I. Utkin, J. Güldner, and J. Shi. Sliding Mode Control in Electromechanical Systems, Florida. CRC Press, 1999.

[28] Nouha Bouchiba. Intégration du générateur à double alimentation dans un réseau isole à énergie éolienne. Doctoral thesis 2018, National Engineering school of Sfax, ENIS Sfax, Tunisia.